Synthesis of Zinc Oxide Nanoparticles on Montmorillonite for Photocatalytic Degradation of Basic Yellow 28: Effect of Parameters and Neural Network Modeling

Murat Kıranşan[1], Alireza Khataee[2]*, Semra Karaca[1],** and Mohsen Sheydaei[3]

[1]Department of Chemistry, Faculty of Science, Atatürk University, 25240 Erzurum, Turkey; [2]Research Laboratory of Advanced Water and Wastewater Treatment Processes, Department of Applied Chemistry, Faculty of Chemistry, University of Tabriz, 51666-16471 Tabriz, Iran; [3]Faculty of Chemistry, Kharazmi University, Tehran, Iran

Abstract: ZnO/montmorillonite (ZnO/MMT) nanocomposite was prepared using MMT as a support, zinc chloride as ZnO synthesis precursor and cetyltrimethylammonium bromide as a surfactant. The prepared ZnO/MMT nanocomposite was characterized by X-ray diffraction, scanning electron microscopy, transmission electron microscope, Fourier transform infrared spectroscopy and N_2 adsorption/desorption analysis. Results indicated the appropriate immobilization of the ZnO nanoparticles with 20-40 nm width on the surface of the MMT. The effect of ZnO immobilization on its adsorption and photocatalytic activity was evaluated by the removal of basic yellow 28 (BY28) in aqueous solution under UV light irradiation. The ZnO/MMT nanocomposite was more effective in adsorption, and photocatalytic degradation processes than pure ZnO. The performance of used light source for photocatalytic degradation of BY28 was found to be in the order of UV-C (wavenumber region of 200-280 nm) > UV-B (wavenumber region of 280-315 nm) > UV-A (wavenumber region of 315-400 nm). An artificial neural network (ANN) model was developed to predict the photocatalytic degradation process under UV-C radiation. The ANN model with reasonable predictive performance ($R^2 = 0.999$) indicated that the influence of initial concentration of BY28 on decolorization process (49.66%) was higher than that of nanocomposite dosage (36.44%) and UV radiation time (13.09%). Results of reusability tests indicated that the ZnO/MMT was stable and appropriate for long time application.

Keywords: Artificial neural network, decolorization, nanocatalyst, photocatalysis, wastewater treatment, ZnO nanoparticles.

1. INTRODUCTION

Synthetic dyes are considered as a major class of organic compounds utilized in various branches of industry such as paper, food, leather and textile [1]. Consequently, considerable amount of these hazardous compounds are discharged into the aquatic environment. Dyes and their destruction intermediate are toxic and carcinogenic compounds and the presence of these compounds in water even at low concentration leads to environmental and aesthetic problems [2]. Therefore, in terms of environment, it is crucial to mineralize these pollutants or convert them to less hazardous products [3]. Numerous efforts have been made by scientific community to generate and utilize appropriate method to remove the organic pollutants from aqueous media. In recent years, advanced oxidation processes (AOPs) have been extensively studied for water and wastewater treatment due to their high efficiency, convenience and environmental compatibility.

AOPs are processes in which inorganic oxidants in the presence of homogeneous or heterogeneous catalysts and under the electrical, chemical or radioactive energy were converted to reactive radicals [4]. AOPs *via* generation of these reactive radicals destruct nearly all organic pollutants and leave no hazardous residues after degradation [5]. On the basis of the energy source, kind of oxidant and catalyst, the AOPs include Fenton, photo-Fenton, photocatalysis, ozonation, UV irradiation, wet oxidation, electrochemical oxidation as well as various combinations of these processes [6-9].

The heterogeneous photocatalytic process has been recognized as a promising approach for the elimination of many organic pollutants. Scientific research in heterogeneous photocatalysis began in the early 1970s [10]. Photocatalysts are a group of semiconductors such as TiO_2, ZnO, ZnS, SnO_2, CdS, NiO and α-Fe_2O_3 which absorbed light energy greater than their band gap and consequently electron (e^-) from valence band (VB) of these compounds is promoted into the conduction band (CB) and hole (h^+) is developed [11, 12]. The produced e^-_{CB} reacts with O_2 during photo-reduction reaction, and h^+_{VB} reacts with H_2O and/or OH^- during photo-oxidation reaction to produce photo-excited reactive species [13].

Among various semi conductors, ZnO and TiO_2 have attracted special attention to be used in photocatalytic

*Address correspondence to these authors at the Research Laboratory of Advanced Water and Wastewater Treatment Processes, Department of Applied Chemistry, Faculty of Chemistry, University of Tabriz, 51666-16471 Tabriz, Iran; Tel: +98 41 33393165; Fax: +98 41 33340191; E-mails: a_khataee@tabrizu.ac.ir (ar_khataee@yahoo.com); **Department of Chemistry, Faculty of Science, Atatürk University, 25240 Erzurum, Turkey; Tel: +90 442 2314435; Fax: +90 442 2360948; E-mails: skaraca@atauni.edu.tr (semra_karaca@yahoo.com)

degradation processes [14]. These semiconductors are relatively inexpensive and stabile compounds with considerable photocatalytic activity [15]. The most important advantage of ZnO over TiO$_2$ is that this semiconductor absorbs over a larger fraction of UV spectrum (<425 nm) in comparison to TiO$_2$ [16]. Accordingly, ZnO has attracted considerable attention to be used as photocatalyst in treatment of polluted water and wastewater [17].

Since photocatalysis is a heterogeneous process, surface area of used semiconductor is an important parameter on efficiency of light absorption and pollutant adsorption. To increase the surface area of a photocatalyst, at least two effective ways have been known. The first one is decreasing the size of photocatalyst and the second one is immobilization of the photocatalyst on the surface of an appropriate adsorbent to combine the advantages of both adsorption and photocatalytic degradation processes. Adsorbent supports the photocatalyst as well as concentrates the pollutants around it to increase the contact of the photogenerated reactive species with pollutants [10-15].

In this work, montmorillonite (MMT) as an appropriate adsorbent was used in support of ZnO. ZnO/MMT composite was prepared through the synthesis of ZnO using the zinc chloride in the presence of MMT. Performance of the synthesized composite was evaluated in the adsorption and photocatalytic degradation processes. Effect of light type including UV-A (wavenumber region of 315-400 nm), UV-B (wavenumber region of 280-315 nm) and UV-C (wavenumber region of 200-280 nm) and photocatalyst dosage on photocatalytic degradation efficiency were studied. A three-layer ANN model using a back propagation algorithm was used to predict the decolorization efficiency of BY28 solution in ZnO/MMT/UV-C process.

2. EXPERIMENTAL PROCEDURE

2.1. Materials

Montmorillonite K10 (MMT) with chemical composition (wt.%) of SiO$_2$ (66.9), Al$_2$O$_3$ (13.8), Fe$_2$O$_3$ (2.8), MgO (1.6), CaO (0.3), Na$_2$O (0.2), and K$_2$O (1.7), cetyltrimethylammonium bromide (CTAB) and other materials were purchased from Sigma-Aldrich Co. (USA). Cation exchange capacity (CEC) of this clay was 120 meq/100g. ZnCl$_2$ was purchased from Merck Co. (Germany). The dye C.I. Basic Yellow 28 (chemical class: Cationic, Methine; molecular formula: C$_{21}$H$_{27}$N$_3$O$_5$S and M$_w$: 433.52 g/mol) was procured from Shimi Boyakhsaz Co. (Iran). All other chemicals were of analytical grade and were used without any further purification. Distilled water was used throughout the investigation.

2.2. Synthesis and Characterization of ZnO/MMT Nanocomposite

In order to synthesize surfactant modified MMT nanomaterial, 1 g MMT was first dispersed in 100 mL distilled water and stirred for 24 h at a stirring speed of 500 rpm to swell and to reach homogeneity. A desired amount of CTAB was slowly added to suspension. The concentration of surfactant was 1.0 CEC of pure MMT. Then, 1 g of zinc chloride was dissolved in 20 mL of distilled water. The pH of the solution

was adjusted to 12.50 using 1 M NaOH solution and a pH meter (Schott- CG840, Germany). Then, it was added to the prepared CTAB/MMT suspension and the prepared mixture was stirred for 6 h. The prepared sample was washed with distilled water and centrifuged. Then, it was taken in an oven for 3 h at 90 °C for drying.

Crystal structures of pure MMT and ZnO particles, and ZnO/MMT composite were determined using X-ray powder diffraction (XRD) measurements by P analytical X'Pert PRO diffractometer (Germany). The radiation source was Cu-Kα with wave number of 0.15406 nm. The applied current was 40 mA and the voltage was 45 kV. Morphology of the samples was investigated using scanning electron microscope (SEM) model MIRA3 FEG-SEM Tescan (Czech) and Cs-corrected high-resolution transmission electron microscope (TEM) model Zeiss-EM10C (Germany) operated at 100 kV. The Fourier transform infrared (FT-IR) spectra of the MMT, ZnO and ZnO/MMT samples were recorded on a Tensor 27, Bruker (Germany) FT-IR spectrometer in a wave number range of 4000–400 cm^{-1} using KBr pellets technique. The pore structure of the MMT, ZnO and ZnO/MMT samples was analyzed with N$_2$ adsorption/desorption isotherms at 77 K on a Gemini 2385 nitrogen adsorption apparatus (Micromeritics Instruments, USA). The Brunauer-Emmett-Teller (BET) equation was used to measure the total specific surface areas (S$_{BET}$), total pore volume (V$_{tot}$) and average pore size (t) [18]. The t-Plot theory was used to calculate the micropore surface area (S$_{mic}$), the external surface area (S$_{ex}$), and the micropore volumes (V$_{mic}$) [19]. Mesopore surface area (S$_{mes}$) was derived from Barrett– Joyner–Halenda (BJH) method [20].

2.3. Decolorization Experiments

2.3.1. Adsorption Experiment

Batch studies were conducted to evaluate the ability of MMT, ZnO and ZnO/MMT samples on adsorption of BY28 as a model contamination. For each adsorption experiment, 500 mL of the BY28 solution of 25 mg/L and desired dosage of the adsorbent were added in a 900-mL cylindrical glass vessel. pH of the solution was adjusted using 1 M HCl or NaOH solutions. The solutions were agitated at constant temperature. At a defined time interval, the samples with volume of 5 mL were withdrawn from the solution and centrifuged for 10 min with 6000 rpm. The residual BY28 concentration (C) was measured using a UV–Vis spectrophotometer (Varian Cary 100 UV-Vis Spectrophotometer, Australia) at maximum wavelength of 439 nm.

2.3.2. Photocatalytic Degradation Experiment

The photocatalytic degradation experiments were conducted in a 900 mL capacity cylindrical glass photoreactor. Artificial irradiation was produced by a 8W UV-A, UV-B or UV-C lamp (Herolab, Germany) which was placed inside a quartz tube within the reactor. The lamp was turned on at the beginning of each experiment. The condition of the experiments was checked and the measurement of BY28 concentration through the degradation process was performed using a procedure similar to the section of 2.3.1.

2.3.3. Artificial Neural Network (ANN)

A three-layered back propagation neural network using Neural Network Toolbox of MATLAB mathematical software was used for the prediction of decolorization efficiency. Linear transfer function (purelin) at hidden and output layer was used. The input variables were ZnO/MMT dosage, dye concentration and UV radiation time in the range of 0.075–0.3 g/L, 10–120 min and 10–120 mg/L, respectively. The decolorization efficiency used as output variable was between 40–98%. The data sets were divided into training, validation and test subsets. All values were normalized in the 0.1–0.9 range using Eq (1):

$$x_i = \frac{0.8(X_i - X_{min})}{(X_{max} - X_{min})} + 0.1 \tag{1}$$

where x_i, X_i, X_{min} and X_{max} are normalized value (i is an index of data), actual experimental value, and minimum and maximum actual experimental values of data sets, respectively.

3. RESULTS AND DISCUSSION

3.1. XRD Analysis

The XRD patterns of the MMT, ZnO and ZnO/MMT samples are illustrated in Fig. (1). The peak at 2 theta of 26.5° of XRD pattern of MMT (JCPDS Card 35-0652) shown in Fig. (1a) corresponds to the interlayer spacing of this clay [21]. X-ray patterns for ZnO and ZnO/MMT nanocomposite reveal the appearance of diffraction peaks at 2 theta of 31.71 (100), 34.41 (002), 36.21 (101), 47.51 (102), 56.61 (110), 63.00 (103), 66.08 (200), 68 (112), and 68.28 (201) consistent with the standard spectrum of hexagonal wurtzite ZnO (JCPDS Card 36-1451) [22, 23]. Presence of diffraction peaks characterizing MMT and ZnO in XRD constitutes a pattern for ZnO/MMT composite indicating the immobilization of ZnO nanoparticles on the surface of MMT. The average thickness of the ZnO crystallites (d) is

calculated using the Debye–Scherrer equation: $d=(k\lambda/\beta\cos\theta)$ where K is the Debye–Scherrer constant (0.89), λ is the X-ray wavelength (0.15406 nm), β is width of the peak with the maximum intensity in half height and θ is the diffraction angle [24]. According to obtained result the average size of the ZnO crystallites in pure ZnO and ZnO/MMT samples are 25 nm.

3.2. SEM and TEM Analysis

The SEM images of the MMT and ZnO, and ZnO/MMT samples are shown in Fig. (2). Fig (2a) shows the MMT flakes with a porous surface. Plate-like ZnO particles are obvious in SEM images of ZnO particles (Fig. 2b), and ZnO/MMT composite (Fig. 2c). Fig. (2c) reveals successful introduction of ZnO into the MMT surface. The averages size of ZnO plates in SEM images was determined using Manual Microstructure Distance Measurement software. Obtained results reveal that both pure and doped ZnO are nanosized with the average width of 20-40 nm. Fig. (2d) is the result of ZnO/MMT EDX analysis, which confirms the coexistence of Si, Zn, O, Al, Mg and K elements in the synthesized nanocomposite. This result indicates the synthesis of ZnO/MMT composite. TEM image of ZnO/MMT nanocomposite indicates that the average size of ZnO nanoparticles were less than 50 nm approving the results obtained from SEM analysis (Fig. 3).

3.3. FT-IR Analysis

The FT-IR spectrum of ZnO shows the characteristic absorption peak at 440 cm^{-1} (Fig. 4b) [23]. Fig. (4a) shows an absorbance spectrum of the pure MMT. The absorbance peaks located at 478 and 545 cm^{-1} correspond to Si-O-Si and Al-O-Si deformation, respectively [25, 26]. The peaks at 785 and 1050 cm^{-1} are characteristic of the Al-O and Si-O stretching vibration, respectively [27, 28]. The peaks disappeared at 1666 and 3460 cm^{-1} are assigned to the stretching vibration of sorbed water and hydroxyl groups [29]. The
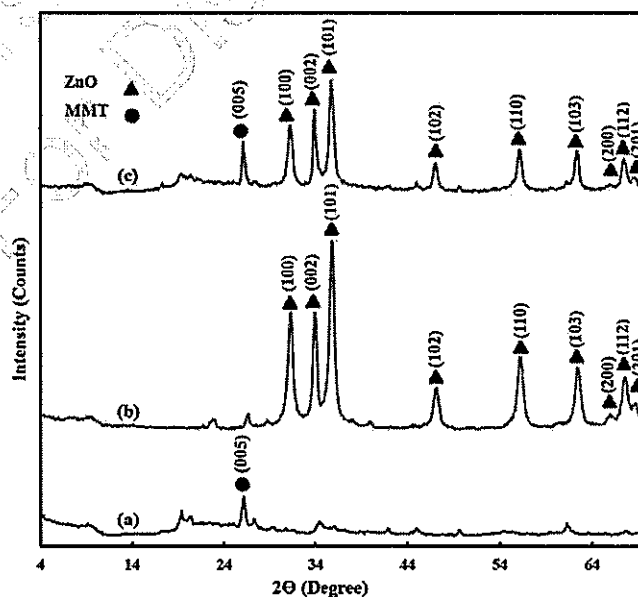

Fig. (1). XRD patterns for (a) the MMT, (b) pure ZnO and (c) ZnO/MMT composite samples.
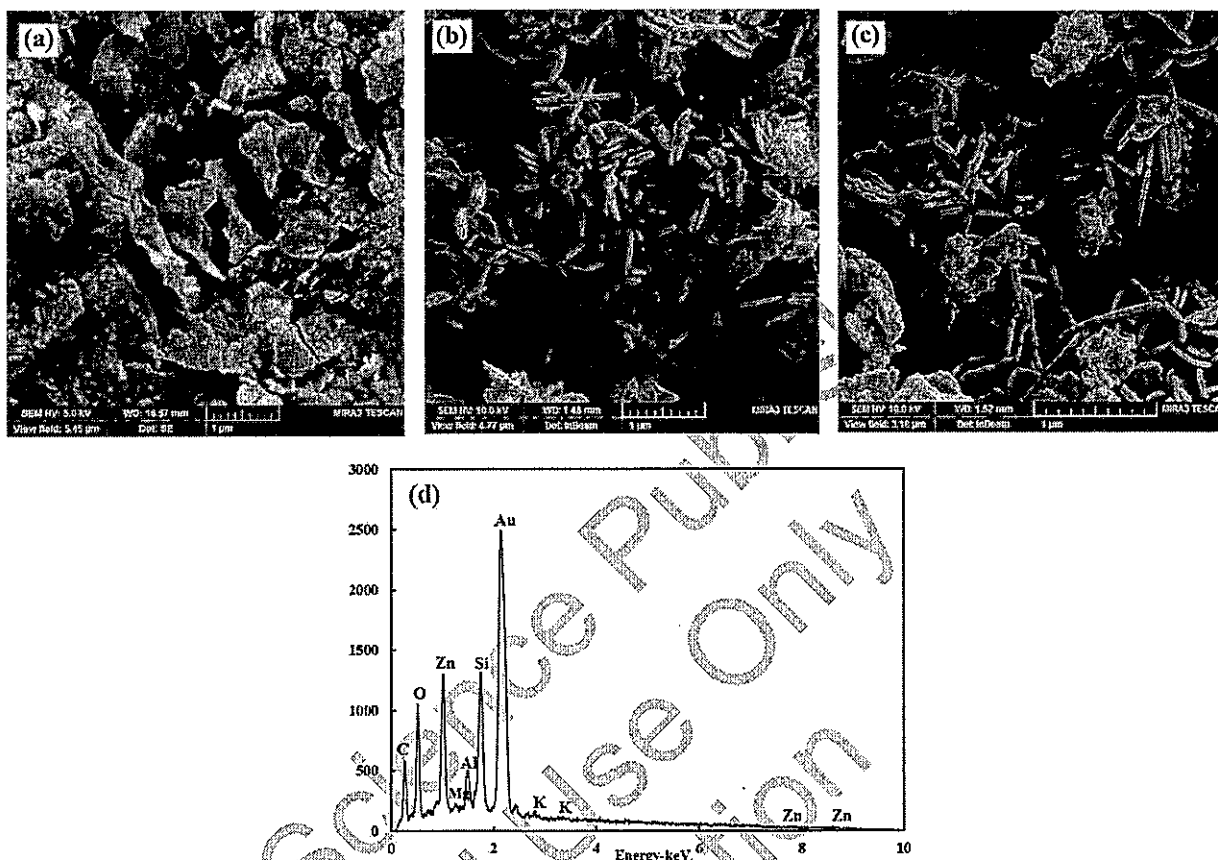
Fig. (2). SEM images of (a) MMT, (b) pure ZnO and (c) ZnO/MMT composite samples, along with (d) EDX micrograph of the synthesized ZnO/MMT sample.

absorption bands located at 2845, 2924 cm^{-1} are attributed to symmetric stretching vibration of C–H and asymmetric stretching vibration of C–H, respectively [30, 31]. Moreover, the peak at 3665 cm^{-1} corresponds to the -OH stretching band of Al-OH and Si-OH [27]. The spectrum of ZnO/MMT shows characteristic absorption peaks of both MMT and ZnO, confirming the development of ZnO/MMT composite.

Fig. (3). TEM image of ZnO/MMT nanocomposite.

3.4. Nitrogen Adsorption/Desorption Analysis

The results obtained from the analysis of nitrogen adsorption/desorption on MMT, ZnO and ZnO/MMT samples with BET, t-plot and BJH methods are summarized in Table 1. The comparison of S_{BET} and V_{tot} of the ZnO and ZnO/MMT samples shows that the surface area and pore volume of prepared composite are nearly two times greater than that of ZnO. Such increase in the surface area and pore volume can promote the adsorption ability. Comparison of the micropore and mesopore surface areas of the ZnO and ZnO/MMT samples obtained from t-Plot and BJH analysis indicates that most of their pores are in mesopore (2- 50 nm) dimensions. As can be seen in Table 1, the average pore size (t) of ZnO/MMT is smaller than that of ZnO. Considering that the adsorption ability of the adsorbent increased with the decrease in pore width, it decreased the pore size of ZnO/MMT rather than that ZnO may enhance the adsorption ability of produced nanocomposite.

3.5. Adsorption of the Dye

3.5.1. Comparison of the Adsorption Ability of ZnO and ZnO/MMT

To investigate the adsorption of BY28 using ZnO and ZnO/MMT samples, the set of adsorption experiments was conducted. Comparing the ability of the adsorbents in the removal of BY28 through the adsorption process indicated that the ZnO/MMT nanocomposite adsorbed more pollutant than pure ZnO (Fig. 5). Higher ability of the ZnO/MMT nanocomposite for BY28 adsorption than that
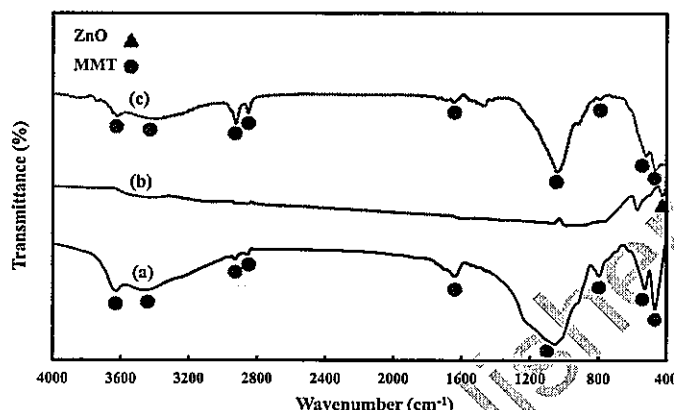
Fig. (4). FT-IR spectra for the (a) MMT, (b) pure ZnO and (c) ZnO/MMT samples.

Table 1. Surface area and porosity characteristics of ZnO, MMT and ZnO/MMT nanocomposite samples.

ZnO/MMT	MMT	ZnO	Sample
70.54	279.28	38.22	S_{BET} (m^2/g)
83.72	272.61	36.22	S_{ex} (m^2/g)
-	6.67	1.99	S_{mic} (m^2/g)
84.98	285.55	32.45	S_{mes} (m^2/g)
0.0000	0.0003	0.0008	V_{mic} (cm^3/g)
0.213-0.228	0.416-0.428	0.217-0.277	V_{tot} (cm^3/g)
12.1-13.0	6.0-6.1	22.7-29.0	t (nm)

of the ZnO nanoparticles is attributed to higher surface area and pore volume of the nanocomposite. Higher adsorption ability of ZnO/MMT nanocomposite compared to pure ZnO would be favorable for the photocatalytic destruction of BY28 over the surface of the ZnO/MMT nanocomposite.

3.5.2. Effect of ZnO/MMT Dosage

The effect of ZnO/MMT dosage (varied from 0.075 to 0.30 g/L) on the BY28 adsorption is shown in Fig. (6). An increase in the dosage of the adsorbent leads to a decrease in the concentration of pollutant in treated solution. This can be attributed to the increased adsorbent surface area and availability of more adsorption sites caused by increasing adsorbent dosage [32]. Similar results have been reported by other researchers [32, 33].
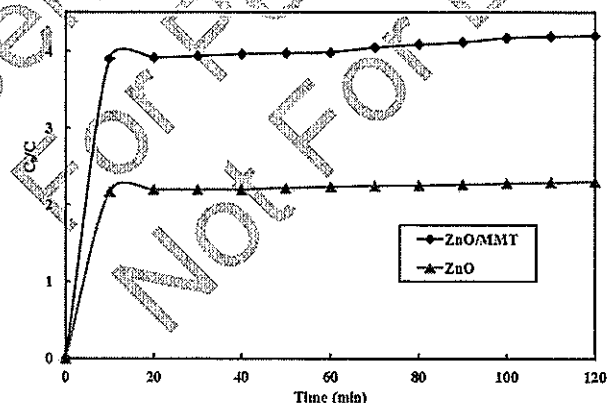

Fig. (5). Evaluation of the adsorption ability of ZnO and ZnO/MMT samples for decolorization of 25 mg/L BY28 solution in the presence of 0.300 g/L adsorbent.
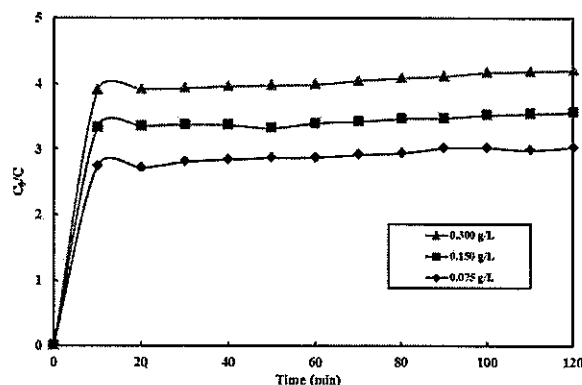

Fig. (6). Effect of ZnO/MMT nanocomposite dosage on the adsorption of BY28 with initial concentration of 25 mg/L.

3.6. Photocatalytic Degradation of BY28

3.6.1. Comparison of the Photocatalytic Performance of ZnO and ZnO/MMT

Effect of ZnO immobilization on the surface of MMT on its photocatalytic behaviors under UV-A, UV-B and UV-C radiation was investigated. Obtained result indicated that under all radiations in UV region, the ability of ZnO/MMT nanocomposite for BY28 removal was higher than that of ZnO nanoparticles (Fig. 7). This indicates that the immobilization of ZnO on the surface of MMT enhanced its photocatalytic performance in all UV radiation range. The increase in the performance of ZnO/MMT rather than ZnO in the decolorization of BY28 solution can be attributed to improved surface area and photocatalytic activity of ZnO/MMT. During photocatalytic degradation of BY28 by UV/ZnO/MMT process, first O_2, H_2O and the organic pollutant are adsorbed on the surface of ZnO/MMT. Simultaneously, UV irradiation photon excites electron from valence band of ZnO to the conduction band, leaving holes in the valence band. The developed electron in the conduction band of TiO_2 may transfer the surface of nanocomposite to react with MMT components (Eq. 2) and/or adsorbed O_2 molecules [34]. This hinders the photo-generated e^-/h^+ recombination and causes further increase in the production of reactive radicals through the reaction of photo-generated h^+ and H_2O. Consequently, produced reactive radicals degrade the adsorbed BY28 molecules and increase the decolorization efficiency.

$$MMT(metals) + e^- \rightarrow MMT(metals)(e^-) \qquad (2)$$

3.6.2. Effect of UV Radiation Region

Fig. (8) shows the ability of ZnO/MMT nanocomposite in the removal of BY28 in the absence and presence of UV-A, UV-B or UV-C lights. The results show the low photocatalytic performance of ZnO/MMT nanocomposite under UV-A light. As can be seen from Fig. (8), the performance of the ZnO/MMT/UV-B process is effective than ZnO/MMT/UV-A process. Among the three UV regions, the highest photocatalytic degradation of BY28 was obtained under UV-C light irradiation which can be attributed to the energy of radiated photon as follow: UV-C (200-280 nm) > UV-B (280-315 nm) >UV-A (315-400 nm) [35]. High energy of the emitted photons in UV-C leads to efficient photogeneration of e^-/h^+ pairs and efficient dye degradation. Similar result has been reported for the degradation of Methyl Orange in aqueous solution under different light irradiation [35].

3.6.3. Effect of ZnO/MMT Dosage

The dosage of the catalyst is one of the important parameters in catalytic reactions. So the effect of ZnO/MMT dosage in the range of 0.075 to 0.300 g/L on photocatalytic degradation of BY28 was investigated. The results have been illustrated in Fig. (9) which shows the increase in dye removal with the increasing photocatalyst dose. This observation can be explained in terms of availability of active sites on the catalyst surface and the penetration of UV light into the suspension. The total photocatalytic active surface area increases with the increasing catalyst dosage which leads to
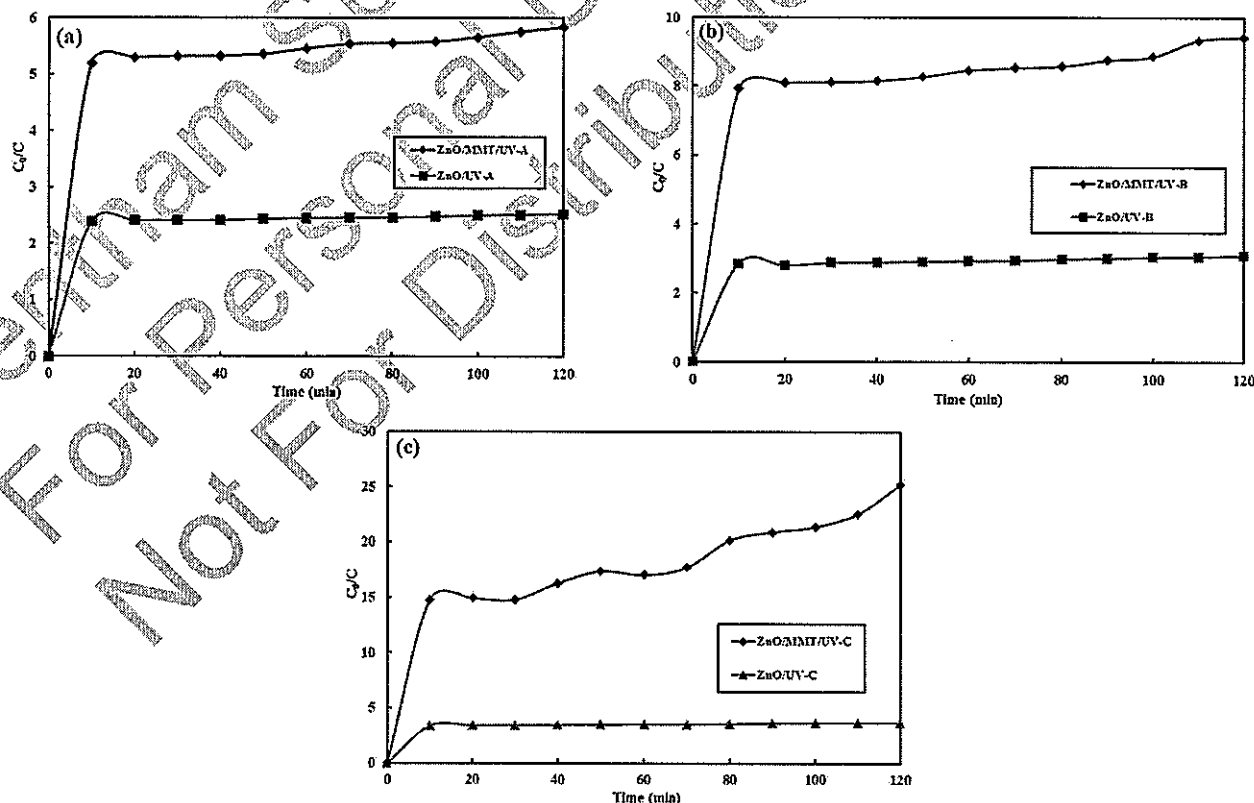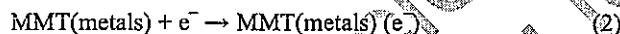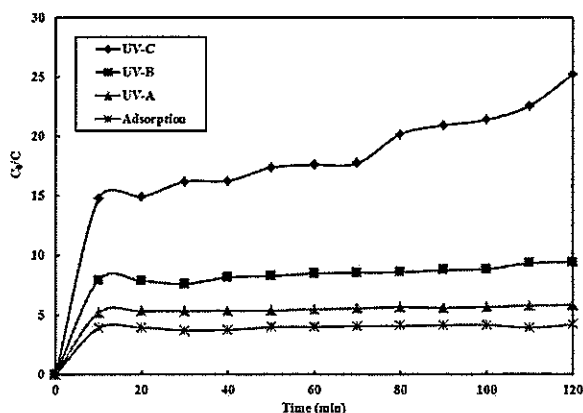

Fig. (7). Evaluation of the photocatalytic performance of ZnO and ZnO/MMT samples for decolorization of 25 mg/L BY28 solution in the presence of 0.300 g/L catalyst under (a) UV-A, (b) UV-B and (c) UV-C radiation.

Fig. (8). Effect of UV radiation region on the degradation of BY28 through photocatalytic degradation process in the presence of ZnO/MMT nanocomposite (Experimental conditions: [ZnO/MMT]₀=0.300 g/L and [BY28]₀= 25 mg/L).
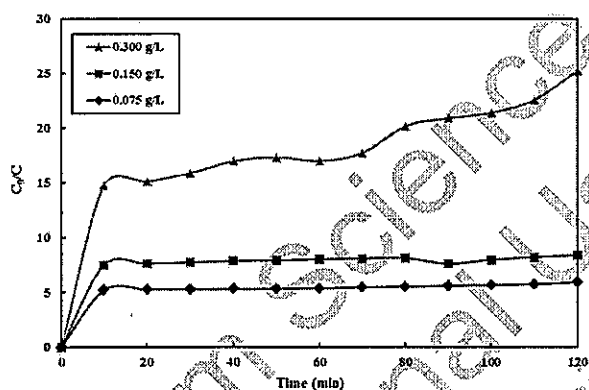

Fig. (9). Effect of ZnO/MMT nanocomposite dosage on the photocatalytic degradation of 25 mg/L BY28 under UV-C light.

the generation of reactive radical [36]. Furthermore, an increase in the surface area of nanocomposite is beneficial for adsorption of BY28 around the photocatalyst sites to effective degradation [37].

3.6.4. Effect of Initial Dye Concentration

Fig. (10) presents the effect of BY28 initial concentration on the C_0/C with ZnO/MMT dose of 0.30 g/L under UV-C radiation. The results showed that the increase in the initial dye concentration led to a decrease in C_0/C value. An increase in the initial dye concentration may decrease the absorbance of UV-A light *via* the catalyst due to absorption of a significant amount of UV light by dye molecules. Furthermore, the increase in dye concentration reduces the path length of photon entering the dye solution and consequently decreases the generation of ‛OH and decolorization efficiency [38].

Langmuir-Hinshelwood (L-H) kinetic equation (Eq. 3) was used to evaluate the kinetic behavior of the photocatalytic degradation of BY28 through the determination of the relationship between the apparent first-order rate constant and the initial concentration of the dye.
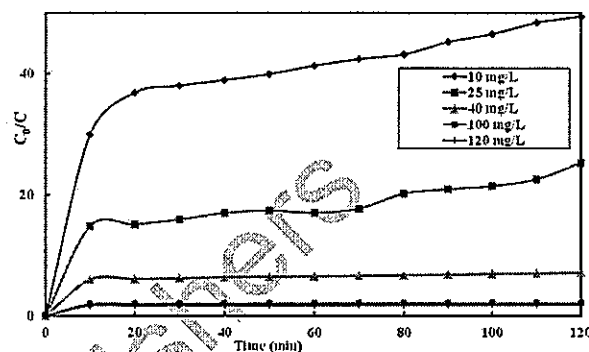

Fig. (10). Effect of BY28 initial concentration on the photocatalytic degradation of this dye in the presence of 0.300 g/L ZnO/MMT nanocomposite under UV-C light.

$$\frac{1}{k_{obs}} = \frac{1}{k_c K_{ads}} + \frac{C_0}{k_c} \tag{3}$$

where C_0, k_{obs}, k_c and K_{ads} are the initial dye concentration (mg/L), observed pseudo-first-order constant, the Langmuir-Hinshelwood rate constant of surface reaction and adsorption equilibrium constant, respectively [39]. As shown in Fig. (11), the data for photocatalytic degradation of BY28 were fitted to Eq. (3), and the resulting values of k_c and K_{ads} obtained were 0.089 mg/L min and 0.107 mg/L, with R^2 value of 0.9626, respectively. These results indicate that the decolorization of BY28 solution using ZnO/MMT nanocomposite was done in two steps. The first step was the adsorption of BY28 on the surface of the nanocomposite and the second step was degradation of dye by photogenerated ‛OH.
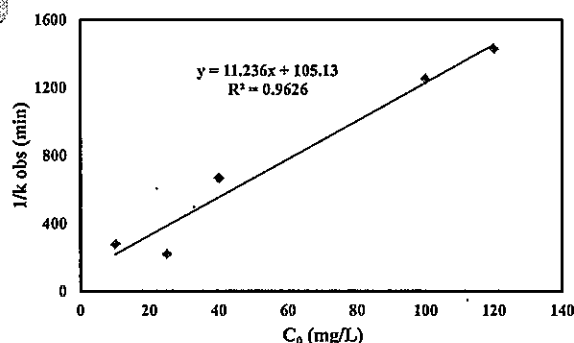

Fig. (11). Variations of $1/k_{app}$ as a function of initial concentration of BY28.

3.6.5. UV-vis Absorption Spectrum Through Photocatalysis

Decolorization experiment has been performed under optimum conditions including [BY28]₀=25 mg/L and [ZnO/MMT]₀=0.300 g/L under UV-C light. UV-vis absorption spectra of all samples which were taken at 10 min intervals up to 120 min were recorded. Obtained results (Fig. 12) show that the maximum peak of 439 nm gradually decreases with irradiation time which indicates the degradation of the studied dye. However, the decrease tendency of the absor-
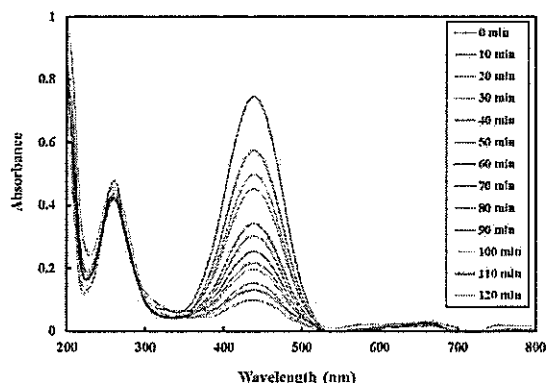
Fig. (12). UV-vis spectrum of synthetic wastewater as a function of photocatalytic reaction time (Experimental conditions: [BY28]$_0$=25 mg/L and [ZnO/MMT]$_0$=0.300 g/L under UV-C radiation).

bance bands appearing in the UV-vis region was low due to the high durability of aromatic groups of the dye.

3.6.6. ANN Modeling

A neural network model consists of input, hidden, and output layers of neuron and the transfer functions between these layers [40]. The number of neurons in the input and output layers is determined by the number of input and output variables. However, selection of appropriate number of neurons in hidden layer is a critical parameter in the performance of developed model. In this work, the optimum number of neurons was determined based on the minimum value of mean square error (MSE) of the training and prediction sets [41]. The optimization was done by varying the neuron number in the range of 2–20. Fig. (13) shows the relationship between number of neurons and MSE. The MSE was decreased with the increase in the number up to 14 and then increased again. Hence, 14 neurons were selected as the best number of neurons for hidden layer.

After the development of the optimized ANN model, the test data set was fed to the developed network in order to test the model. Comparison between the experimental decolorization efficiency and predicted values using the neural network model (Fig. 14) shows the good performance of ANN model in prediction of experimental data within the adopted ranges with correlation coefficient (R^2) of 0.999. Set of connection weights and biases that cause the optimum ANN topography
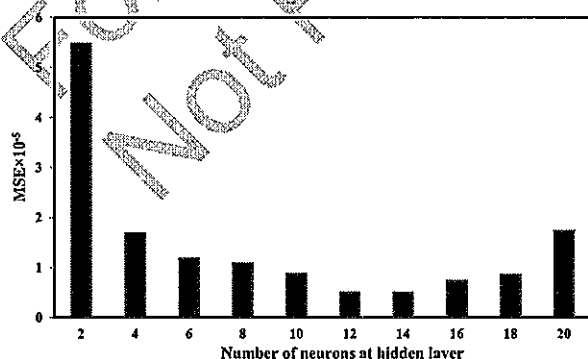

Fig. (13). Dependence between MSE and number of neurons at hidden layer.

is listed in Table 2. To determine the relative importance of the ZnO/MMT dosage, dye concentration and UV radiation time variables, Garson equation (Eq. 4) was used [42]:

$$I_j = \frac{\sum\limits_{m=1}^{m=N_h} ((|W_{jm}^{ih}| / \sum\limits_{k=1}^{k=N_i} |W_{km}^{ih}|) \times |W_{mn}^{ho}|)}{\sum\limits_{k=1}^{k=N_i} \{\sum\limits_{m=1}^{m=N_h} ((|W_{jm}^{ih}| / \sum\limits_{k=1}^{N_i} |W_{km}^{ih}|) \times |W_{mn}^{ho}|)\}} \tag{4}$$

where I_j is the relative importance of the j_{th} input variable on the output variable, N is the number of neurons, and W is connection weight. The superscripts 'i', 'h' and 'o' refer to input, hidden and output layers, respectively and subscripts 'k', 'm' and 'n' refer to input, hidden and output neurons, respectively. According to the obtained results, the relative importance of ZnO/MMT dosage, dye concentration and UV radiation time variables on decolorization efficiency were 36.44, 49.66 and 13.9%, respectively.
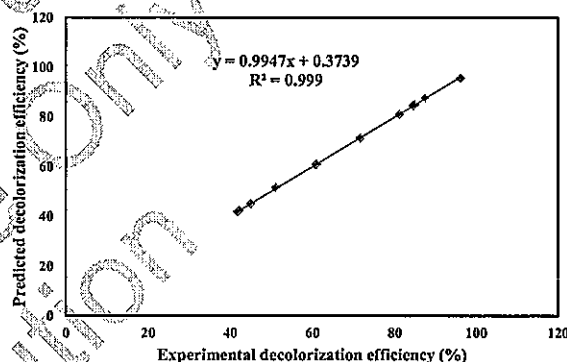

Fig. (14). Predicted result vs. experimental result for decolorization efficiency.

3.6.7. Reusability of the ZnO/MMT

To evaluate the reusability of the ZnO/MMT nanocomposite, successive batches experiments of BY28 degradation with initial concentration of 25 mg/L in the presence of 0.30 g/L catalyst under UV-C radiation were performed. The results showed that photocatalytic behavior of ZnO/MMT nanocomposite was reproducible in successive experiments without a remarkable decrease in the process performance (Fig. 15). These results indicate that the ZnO/MMT photocatalyst is stable and appropriate for long time application.
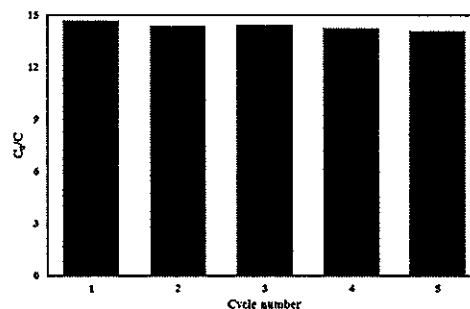

Fig. (15). Reusability behavior of ZnO/MMT in Photocatalytic decolorization of BY28 solutions (Experimental conditions: [BY28]$_0$=25 mg/L and [ZnO/MMT]$_0$=0.300 g/L under UV–C radiation).

Table 2.　Matrices of ANN optimized structure weights and biases.

Weights and biases between input and hidden layers				
Neuron of hidden layer	Variable			Bias
	ZnO/MMT dosage	UV radiation time	Initial concentration of BY28	
1	2.05	0.51279	-3.0894	3.4497
2	0.67075	0.26197	3.6528	3.6694
3	1.5612	0.94329	2.6436	2.8833
4	1.0711	1.3927	2.7499	1.6182
5	0.67183	0.32207	0.62691	2.0017
6	1.2502	0.38211	2.41	0.38014
7	3.1833	0.87985	1.2311	0.29381
8	1.5956	0.094096	3.318	1.137
9	2.9021	1.2376	0.81757	1.1696
10	2.6236	0.91137	2.734	1.2705
11	2.4136	1.2702	2.1441	1.7165
12	3.0043	1.2707	1.7024	2.5523
13	0.60229	2.7184	0.89686	2.3525
14	1.1588	2.2324	1.8846	3.528
Weights and bias between hidden and output layers				
Neuron of hidden layer	Weights		Bias	
1	0.18674		0.23911	
2	1.8648			
3	0.10549			
4	0.020326			
5	2.33			
6	0.37472			
7	0.75036			
8	0.94843			
9	0.029576			
10	1.2799			
11	0.049198			
12	0.92445			
13	0.047228			
14	0.06577			

4. CONCLUSIONS

A simple approach was introduced to synthesize ZnO/MMT composite containing ZnO nanoparticles of 20-40 nm distributed on MMT surface. The immobilization of ZnO nanoparticles on the surface of MMT led to an increase in its adsorption and photocatalytic degradation performance. The effect of UV region on the degradation of BY28 was found to be in the order of: UV-C > UV-B > UV-A. Increase in the dosage of nanocomposite enhanced the dye removal through both adsorption and photocatalytic degradation processes. The results of ANN modeling confirmed that

obtained model could effectively reproduce experimental data and predict the behavior of the process. In addition, the possibility of cyclic usage of the prepared photocatalyst was confirmed.

CONFLICT OF INTEREST

The authors confirm that this article content has no conflict of interest.

ACKNOWLEDGEMENTS

REFERENCES

[1]   Aber, S.; Sheydaei, M. Application of physicochemically prepared activated carbon fiber for the removal of basic blue 3 from water. *Desal. Water Treat.*, 2011, *28*(1-3), 97-102.

[2]   Sheydaei, M.; Aber, S.; Khataee, A. Preparation of a novel γ-FeOOH-GAC nano composite for decolorization of textile wastewater by photo Fenton-like process in a continuous reactor. *J. Mol. Catal. A: Chem.*, 2014, *392*(0), 229-234.

[3]   Khataee, A.; Akbarpour, A.; Vahid, B. Photoassisted electrochemical degradation of an azo dye using Ti/RuO₂ anode and carbon nanotubes containing gas-diffusion cathode. *J. Taiwan Inst. Chem. Eng.*, 2014, *45*(3), 930-936.

[4]   Vilar, V.J.P.; Capelo, S.M.S.; Silva, T.; Boaventura, R.A.R. Solar photo-Fenton as a pre-oxidation step for biological treatment of landfill leachate in a pilot plant with CPCs. *Catal. Today*, 2011, *161*(1), 228-234.

[5]   Ayoubi-Feiz, B.; Aber, S.; Khataee, A.; Alipour, E. Electrosorption and photocatalytic one-stage combined process using a new type of nanosized TiO₂/activated charcoal plate electrode. *Environ. Sci. Pollut. Res.*, 2014, *21*(14), 8555-8564.

[6]   Sheydaei, M.; Aber, S.; Khataee, A. Degradation of amoxicillin in aqueous solution using nanolepidocrocite chips/H₂O₂/UV: Optimization and kinetics studies. *J. Ind. Eng. Chem.*, 2013, *20*, 1772-1778.

[7]   Khataee, A.; Vatanpour, V.; Amani Ghadim, A. Decolorization of C.I. Acid Blue 9 solution by UV/Nano-TiO₂/Fenton, Fenton-like, electro-Fenton and electrocoagulation processes: A comparative study. *J. Hazard. Mater.*, 2009, *161*(2), 1225-1233.

[8]   Khataee, A.R.; Amani-Ghadim, A.R.; Rastegar Farajzade, M.; Valinazhad Ourang, O. Photocatalytic activity of nanostructured TiO₂-modified white cement. *J. Exper. Nanosci.*, 2011, *6*(2), 138-148.

[9]   Khataee, A.R.; Zarei, M.; Moradkhannejhad, L. Application of response surface methodology for optimization of azo dye removal by oxalate catalyzed photoelectro-Fenton process using carbon nanotube-PTFE cathode. *Desalination*, 2010, *258*, 112-119.

[10] Zhang, W.; Zou, L.; Wang, L. Photocatalytic TiO₂/adsorbent nanocomposites prepared via wet chemical impregnation for wastewater treatment: A review. *Appl. Catal., A*, 2009, *371*(1-2), 1-9.

[11] Pourata, R.; Khataee, A.R.; Aber, S.; Daneshvar, N. Removal of the herbicide Bentazon from contaminated water in the presence of synthesized nanocrystalline TiO₂ powders under irradiation of UV-C light. *Desalination*, 2009, *249*(1), 301-307.

[12] Motahari, F.; Mozdianfard, M.R.; Soofivand, F.; Salavati-Niasari, M. NiO nanostructures: synthesis, characterization and photocatalyst application in dye wastewater treatment. *RSC Advances*, 2014, *4*(53), 27654-27660.

[13] Khataee, A.R.; Aleboyeh, H.; Aleboyeh, A. Crystallite phase-controlled preparation, characterisation and photocatalytic properties of titanium dioxide nanoparticles. *J. Exper. Nanosci.*, 2009, *4*(2), 121-137.

[14] Khataee, A.R.; Fathinia, S.; Fathinia, M.; Hanifehpour, Y.; Joo, S.W.; Soltani, B. Synthesis, characterization and photocatalytic

[15] properties of nanostructured Sm-doped CdSe. *Curr. Nanosci.*, 2013, *9*(6), 780-786.

[15] Senthilraja, A.; Subash, B.; Krishnakumar, B.; Rajamanickam, D.; Swaminathan, M.; Shanthi, M. Synthesis, characterization and catalytic activity of co-doped Ag-Au-ZnO for MB dye degradation under UV-A light. *Mater. Sci. Semicond. Process.*, 2014, *22*(0), 83-91.

[16] Nezamzadeh-Ejhieh, A.; Khorsandi, S. Photocatalytic degradation of 4-nitrophenol with ZnO supported nano-clinoptilolite zeolite. *J. Ind. Eng. Chem.*, 2014, *20*(3), 937-946.

[17] Akyol, A.; Bayramoglu, M. Performance comparison of ZnO photocatalyst in various reactor systems. *J. Chem. Technol. Biotechnol.*, 2010, *85*(0), 1455-1462.

[18] Brunauer, S.; Emmett, P.H.; Teller, E. Adsorption of gases in multimolecular layers. *J. Am. Chem. Soc.*, 1938, *60*(2), 309-319.

[19] Lippens, B.C.; de Boer, J.H. Studies on pore systems in catalysts: V. The t method. *J. Catal.*, 1965, *4*(3), 319-323.

[20] Barrett, E.P.; Joyner, L.G.; Halenda, P.P. The determination of pore volume and area distributions in porous substances. I. computations from nitrogen isotherms. *J. Am. Chem. Soc.*, 1951, *73*(1), 373-380.

[21] Rasouli, F.; Aber, S.; Salari, D.; Khataee, A.R. Optimized removal of Reactive Navy Blue SP-BR by organo-montmorillonite based adsorbents through central composite design. *Appl. Clay Sci.*, 2014, *87*(0), 228-234.

[22] Khataee, A.; Darvishi Cheshmeh Soltani, R.; Hanifehpour, Y.; Safarpour, M.; Gholipour Ranjbar, H.; Joo, S.W. Synthesis and characterization of dysprosium-doped ZnO nanoparticles for photocatalysis of a textile dye under visible light irradiation. *Ind. Eng. Chem. Res.*, 2014, *53*(5), 1924-1932.

[23] Liu, H.; Yang, J.; Liang, J.; Huang, Y.; Tang, C. ZnO nanofiber and nanoparticle synthesized through electrospinning and their photocatalytic activity under visible light. *J. Am. Ceram. Soc.*, 2008, *91*(4), 1287-1291.

[24] Sheydaei, M.; Aber, S. Preparation of nano-lepidocrocite and an investigation of its ability to remove a metal complex dye. *CLEAN - Soil, Air, Water*, 2013, *41*(9), 890-898.

[25] Tajeddine, L.; Mountacer, H.; Sarrakha, M. Effect of iron and humic acid on photodegradation of some pesticides adsorbed on clay surfaces. *Arab. J. Chem.*, 2010, *3*(2), 73-78.

[26] Khataee, A.; Bozorg, S.; Vahid, B.; Dang, T.-D.; Hanifehpour, Y.; Joo, S.W. Synthesis and Immobilization of MnO₂ Nanoparticles on Bio-silica for the Efficient Degradation of an Azo Dye in the Aqueous Solution. *Curr. Nanosci.*, 2015, *11*(1), 129-134.

[27] Shirzad-Siboni, M.; Farrokhi, M.; Darvishi Cheshmeh Soltani, R.; Khataee, A.; Tajassosi, S. Photocatalytic reduction of hexavalent chromium over ZnO nanorods immobilized on kaolin. *Ind. Eng. Chem. Res.*, 2014, *53*(3), 1079-1087.

[28] Khataee, A.; Sheydaei, M.; Hassani, A.; Taseidifar, M.; Karaca, S. Sonocatalytic removal of an organic dye using TiO₂/Montmorillonite nanocomposite. *Ultrason. Sonochem.*, 2015, *22*(0), 404-411.

[29] Karaca, S.; Gürses, A.; Ejder Korucu, M. Investigation of the orientation of CTA⁺ ions in the interlayer of CTAB pillared montmorillonite. *J. Chem.*, 2013, *2013*(0), 1-10.

[30] Aber, S.; Khataee, A.; Sheydaei, M. Optimization of activated carbon fiber preparation from Kenaf using K₂HPO₄ as chemical activator for adsorption of phenolic compounds. *Bioresour. Technol.*, 2009, *100*(24), 6586-6591.

[31] Soofivand, F.; Mohandes, F.; Salavati-Niasari, M. Silver chromate and silver dichromate nanostructures: Sonochemical synthesis, characterization, and photocatalytic properties. *Mater. Res. Bull.*, 2013, *48*(6), 2084-2094.

[32] Asl, S.H.; Ahmadi, M.; Ghiasvand, M.; Tardast, A.; Katal, R. Artificial neural network (ANN) approach for modeling of Cr(VI) adsorption from aqueous solution by zeolite prepared from raw fly ash (ZFA). *J. Ind. Eng. Chem.*, 2013, *19*(3), 1044-1055.

[33] Bhaumik, M.; Leswifi, T.Y.; Maity, A.; Srinivasu, V.V.; Onyango, M.S. Removal of fluoride from aqueous solution by polypyrrole/Fe₃O₄ magnetic nanocomposite. *J. Hazard. Mater.*, 2011, *186*(1), 150-159.

[34] Tahir, M.; Amin, N.S. Photocatalytic reduction of carbon dioxide with water vapors over montmorillonite modified TiO₂ nanocomposites. *Appl. Catal., B*, 2013, *142-143*, 512-522.

[35] Han, H.; Bai, R. Effect of thickness of photocatalyst film immobilized on a buoyant substrate on the degradation of methyl orange

dye in aqueous solutions under different light irradiations. *Ind. Eng. Chem. Res.*, 2011, *50*(21), 11922-11929.

[36]   Fatimah, I.; Wang, S.; Wulandari, D. ZnO/montmorillonite for photocatalytic and photochemical degradation of methylene blue. *Appl. Clay Sci.*, 2011, *53*(4), 553-560.

[37]   Shirzad-Siboni, M.; Khataee, A.; Vahid, B.; Joo, S.W.; Fallah, S. Preparation of a Green Photocatalyst by Immobilization of Synthesized ZnO Nanosheets on Scallop Shell for Degradation of an Azo Dye. *Curr. Nanosci.*, 2014, *10*(5), 684-694.

[38]   Khataee, A.R. Photocatalytic removal of C.I. Basic Red 46 on immobilized TiO₂ nanoparticles: artificial neural network modelling. *Environ. Technol.*, 2009, *30*(11), 1155-1168.

[39]   Daneshvar, N.; Rasoulifard, M.H.; Khataee, A.R.; Hosseinzadeh, F. Removal of C.I. Acid Orange 7 from aqueous solution by UV irra-

diation in the presence of ZnO nanopowder. *J. Hazard. Mater.*, 2007, *143*(1-2), 95-101.

[40]   Khataee, A.R.; Zarei, M.; Pourhassan, M. Application of microalga Chlamydomonas sp. for biosorptive removal of a textile dye from contaminated water: modelling by a neural network. *Environ. Technol.*, 2009, *30*(14), 1615-1623.

[41]   Khataee, A.R.; Zarei, M.; Dehghan, G.; Ebadi, E.; Pourhassan, M. Biotreatment of a triphenylmethane dye solution using a Xanthophyta alga: Modeling of key factors by neural network. *J. Taiwan Inst. Chem. Eng.*, 2011, *42*(3), 380-386.

[42]   Khataee, A.; Marandizadeh, H.; Zarei, M.; Aber, S.; Vahid, B.; Hanifehpour, Y.; Joo, S.W. Treatment of an Azo Dye by Citrate Catalyzed Photoelectro-Fenton Process Under Visible Light using Carbon Nanotube-polytetrafluoroethylene Cathode. *Curr. Nanosci.*, 2013, *9*(3), 387-393.